5th International Conference on Biaxial/Multiaxial Fatigue and Fracture
Cracow'97, Poland

Jürgen MEERSMANN, Holger FRENZ, Josef ZIEBS*,
Hellmuth KLINGELHÖFFER, Hans-Joachim KÜHN,

Thermomechanical Deformation Behaviour of IN 738 LC and SC 16

Bundesanstalt für Materialforschung und –prüfung (BAM)
Unter den Eichen 87, D – 12205 Berlin, Germany

Keywords: Multiaxial thermomechnical fatigue, IN 738 LC, SC 16, life prediction

ABSTRACT: This article describes the study of uniaxial and biaxial thermo-mechanical fatigue (TMF) response of IN 738 LC and the initial experiments of single crystal superalloy SC 16. A life prediction assessment is proposed based on the inelastic work $\sum \sigma_{ij} \Delta \varepsilon_{ij}^{in}{}'$ *at* $N_f/2$. *It is shown that the* J_2*-theory is applicable to TMF-loadings. Initial experiments on single crystal superalloy SC 16 prove that there is a non-uniform strain distribution in the plastic region along the circumference of [001] orientated specimens. These findings must be weighed when performing TMF-tests.*

Introduction

High temperature energy system components will often experience inelastic deformation resulting from mechanical loading, thermal transient cycles, and thermal gradients. Such forms of multiaxial thermomechanical fatigue (TMF) can involve damage mechanisms that differ significantly from those in isothermal fatigue. To understand these mechanisms, it is imperative that simple and simulated in service thermomechanical cycling should be explored.

The main purpose of the research reported in this paper is to develop a model to predict the TMF life of industrial gas turbine blades for multiaxial loading. TMF data for IN 738 LC under uniaxial loading has been given by Russel (1), Kuwabara et al. (2) and by Bernstein et al (3). The model developed is a semi-empirical model, similar to most engineering

* Corresponding author

models that are actually used to predict low cycle fatigue. A secondary objective of this research is to better understand the multiaxial TMF behaviour of IN 738 LC and SC 16. Concerning the single crystal superalloy SC 16 the main features of the deformation behaviour are the anisotropic (structural and induced by the plastic flow) and inhomogeneous effects. A further objective of this research is to demonstrate how experimental results can give guidance to the development of time and temperature dependent constitutive models.

Materials Details and Experimental Procedures

The materials studied were the cast nickel base alloys IN 738 LC and SC 16. The chemical composition and the heat treatment of the alloys are presented in **Table 1**.

Table 1. Chemical Composition of IN 738 LC and SC 16

C	Cr	Co	Mo	Ta	Ti	Al	W	Si	Mn	Nb	Fe	Zn
						IN 738 LC						
0.105	15.99	8.7	1.77	1.9	3.45	3.4	2.71	0.09	0.03	0.82	0.3	0.037
	Solution treated at 1120 °C for 2 h, air cooled, aged at 850 °C for 24 h.											
						SC 16						
0.01	15.4	0.17	2.8	3.5	3.48	3.45			<0.003	<0.003		
	Solution treated at 1260 °C for 2 h, vacuum, high-temperature aging at 1100 °C for 4 h, final aging at 850 °C for 24 h, then finally air cooled.											

The test program comprised two groups of experiments: 1. uniaxial and tension-torsion thermomechanical fatigue with linear, diamond and sinusoidal cycling (simple TMF-tests) and 2. complex "bucket" uniaxial and tension-torsion thermo-mechanical tests. As can be seen in **Table 2** the simple TMF-tests differ in the ε/γ-ratio, in the ε/T-and ε/γ-paths: tension-compression-tests with ε/T phase angles $\varphi_T = 0°$, linear in phase (IP) and 180° out of phase (180 OP) and diamond ε/T-cyclings, $\pm$ 90° (OP); torsion tests with γ/T phase angles $\varphi_T = 0°$ (IP) and $\varphi_T = 90°$ (OP) diamond and circular cycling; proportional tension-torsion tests with ε/T and γ/T phase angles $\varphi_T = 0°$ (IP) and $\pm$ 90° (OP) s inusoidal and

Table 2. Details of simple and complex thermomechanical strain paths

Temperature °C			Temperature rate K s^{-1}		Phase angle °		Strain versus temperature
T_1	T_2	T_s	$\dot{\varepsilon} = 10^{-4}s^{-1}$	$\dot{\varepsilon} = 10^{-5}s^{-1}$	ε - T	γ - T	
TMF Tensile-compressive strain			ε_m = 0,6 %, 0,5 %, 0,4 % (CCD, CWD ε_m = 0,6 %)				
950	450	700	4,17	0,42	0, 180		
850	600	725	2,08	0,21	0, 180		
750	550	650	1,67	0,17	0, 180		
950	450	450	4,17		-90		
850	600	600	2,08		-90		
450	950	950	4,17		90		
600	850	850	2,08		90		
TMF Shear strain			$\gamma/\sqrt{3}$ = 0,6 %, $\dot{\gamma}/\sqrt{3} = \dot{\varepsilon}$				
950	450	700	4,17	0,42		0, 90	
760	450	605	2,58	0,26		0, 90	
450	950	950	4,17	0,42		90	
450	760	760	2,58	0,26		90	
TMF Proportional axial and shear strain ε_m = 0,6 %							
950	450	700	4,17	0,42	0	0	
760	450	605	2,58	0,26	0	0	
450	950	700	4,17		-90	-90	
450	950	950	4,17	0,42	90	90	
450	760	760	2,58	0,26	90	90	
TMF Nonproportional axial and shear strain ε_m = 0,4 %, 0,5 %, 0,6 %							
450	950	700	4,17		180	-90	
600	850	725	2,08		180	-90	

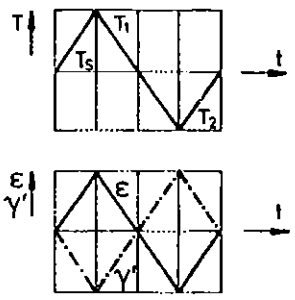

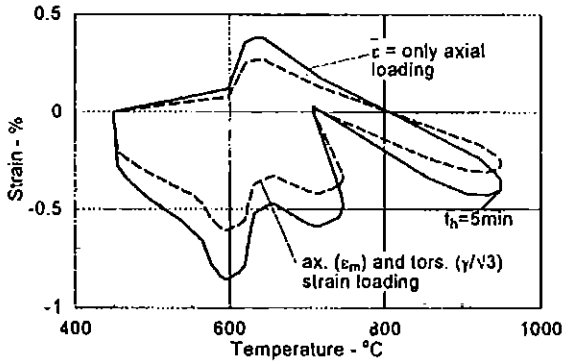

Complex TMF-paths

diamond cycling; non-proportional tension-torsion tests with ε/T phase angles φ_T = 180° and γ/T phase angles φ_T = -90° (diamond, sinusoidal).

The complex "bucket" thermo-mechanical fatigue tests followed an assumed strain-temperature history representative of the leading edge of the first stage bucket in service. The tests were performed at equivalent strain ranges $\Delta\bar{\varepsilon}_m$ = 0.6 %, 0.93 %, 1.24 %, equivalent strain rate $\dot{\bar{\varepsilon}}_m = 10^{-4}s^{-1}, 10^{-5}s^{-1}$, the temperature range 450 °C < T < 950 °C and temperature rate $\dot{T} = 1.67, 2.08, 2.58$ and $4.21\,Ks^{-1}$.

An effective stress range $\Delta\bar{\sigma}$ and an effective plastic strain range $\Delta\bar{\varepsilon}$ based on the von Mises criterion were used for correlating the multiaxial tension/torsion cyclic data:

$$\Delta\bar{\sigma} = \left[(\Delta\sigma)^2 + 3(\Delta\tau)^2\right]^{1/2} \tag{1}$$

and

$$\Delta\bar{\varepsilon} = \left[(\Delta\varepsilon_m)^2 + \frac{1}{3}(\Delta\gamma)^2\right]^{1/2} \tag{2}$$

where Δσ and Δτ are the axial stress and shear stress ranges, respectively. $\Delta\varepsilon_m$ and Δγ are the corresponding components of the axial and shear strain ranges.

Total specimen strain ε_{tot} was calculated by adding thermal ε_{th} and mechanical strain ε_m. The thermal strain was determined by

$$\varepsilon_{th} = \alpha\,(T)\,(T - T_o) \tag{3}$$

where T is the instantaneous Temperature, T_o = 20 °C and α the coefficient of thermal expansion. Based on experimental data α (T) could be approximated by

$$\alpha(T) = A_1 + A_2(T - T_o) + A_3(T - T_o)^2 \tag{4}$$

where A_1, A_2, A_3 are constants.

Details of the corresponding isothermal low cycle fatigue data along with the cyclic hardening and softening behaviour can be found in (4).

Monotonous and sequential tension, torsion and tension-torsion loadings have been performed along <001> and within the standard triangle type orientations on hollow speci-

mens of SC 16 to demonstrate the various aspects of non-homogeneous deformation. Eight or seven strain gauge rosettes have been attached on the circumference of the cross section with respect to the orientation of the axis at RT. Each strain gauge had dimensions of 0.76 x 0.76 mm. The tests were conducted under axial and torsional strain or displacement (stroke) and angle position control.

Life Prediction Results

The simple TMF experiments were designed to investigate three points. Firstly, strain-temperature phase effects were studied by using in-phase, out-of-phase and diamond TMF cycles, where the axial strain, shear strain or the axial and shear strain amplitude were held constant, $\varepsilon_m = \bar{\varepsilon} = \pm 0.4$, 0.5 and 0.6 %. Does this result in different fatigue lives? Secondly, how do different temperature ranges 450 °C - 950 °C, 450 °C – 760 °C and 600 °C – 850 °C affect fatigue lives? Thirdly, can the isothermal data and the J_2-theory be used to describe the thermo-mechanical response of IN 738 LC?

The longest lives in air were exhibited by those samples which had undergone diamond-type loadings (5). For those tests, the strain at the maximum temperature was zero. The shortest lives were seen in those tested under sinusoidal non-proportional strain paths.

Different temperature mechanical strain phasings, that is linear out-of-phase or in phase cycling, had a significant effect in fatigue lives in the temperature range 450 °C to 950 °C. A crossover of the linear TMF lines with temperature phasing of 0° or 180° is seen at about 10 cycles to failure, **Figure 1**. The linear out-of-phase TMF cycle best simulates the complex blade TMF cycle for uniaxial loading (axial strain) because the highest temperatures occurs while the surface is in compression. Nevertheless more damaging thermal mechanical loading was found in sinusoidal tension-torsion cycles with or without hold times. On the other hand complex TMF tests gave longer lives at low strain ranges when compared with simple linear TMF tests. Since the high temperature deformation for complex TMF tests occurs at larger compressive inelastic strain, a shift in mean stress is seen in all tests.

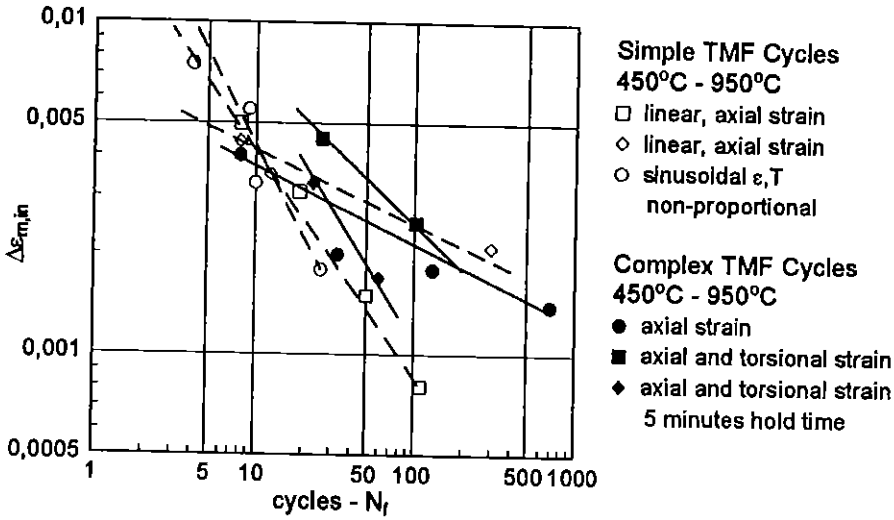

Fig.1 Inelastic strain range, $\Delta\varepsilon_{in,\,in}$, versus cycles to failure for simple and complex TMF tests of IN 738 LC, $\dot{\bar{\varepsilon}} = 10^{-4}\,s^{-1}$

The fatigue life was found to be mainly spent in the propagation of microcracks as for isothermal tests. Fatigue lives for the different TMF cycles are significantly less than for isothermal cycles at the same maximum temperature (4). This suggests that the thermal cycling introduces additional damage associated with thermal inhomogenities, either microscopically or macroscopically.

Linear TMF tests conducted in the temperature range 450 °C to 750 °C gave longer lives, that is twice more than the tests with the temperature range 450 °C to 950 °C (4). However, the environmental attack should also be considered because it is greater at higher temperatures.

The applied axial-torsional strain temperature history for proportional tension-torsion, non-proportional diamond and complex "bucket" loadings and the resulting axial and shear stress temperature/cycles to failure responses are presented in **Figure 2**.

The applied in-phase (φ_T = 0°) proportional strain-temperature path results in an asymmetric stress response (**Figure 2 a**). In the range of high temperatures, 750 °C to 950 °C, a significant stress relaxation is observed due to dynamic recovery. The stress response for tension and torsion is similar.

The non-proportional diamond (φ_T = 90 °) strain-temperature path achieves extremes of strain at T = 700 °C, **Figure 2 b**. The TMF stress response meets at comparable mechanical

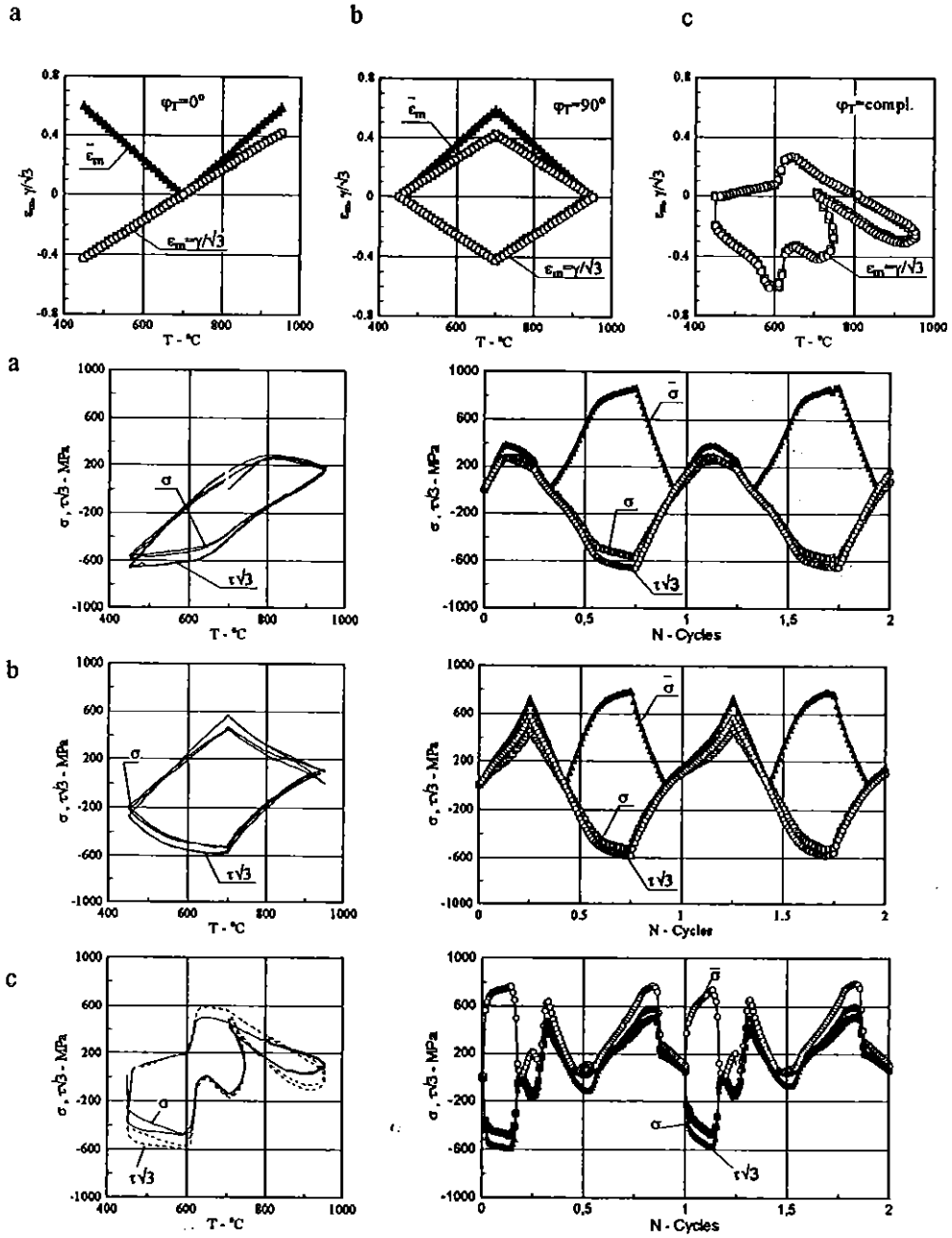

Fig. 2 Applied strain and temperature phasings and stress responses for simple and complex TMF tests

strains the response of isothermal tests in the temperature range 700 °C to 450 °C to 700 °C. In the 850 °C to 950 °C to 850 °C range softening is observed.

As shown in **Figure 2 c** compressive stress peaks occur after warm-up, during acceleration and at base load for the blade strain temperature cycles. Tensile peaks occur before 'load' and during 'unload'. The largest inelastic strain is achieved after warm up. It is mainly reduced during the unload phase by tensile stress. The effects of different strain ranges ($\Delta\varepsilon$ = 1.24 %, 0.93 %, 0.60 %) upon the fatigue lives is shown in **Figure 3** for the complex bucket cycle. Peak stresses ($\overline{\sigma}$, σ_{max}, σ_{min}, τ_{max} ,τ_{min}) are plotted versus the number of cycles. The hardening/softening behaviour is similar to the behaviour of the isothermal counterparts. However, the different strain ranges generate increasing tensile mean stresses. The effect of these tensile mean stresses on fatigue life typically increases as the total strain range increases. Note that the simple TMF tests generate compressive mean stresses in the hysteresis loops (**Figure 2**). However the magnitudes of these compressive mean stresses are relatively small in comparison to magnitudes of those generated in the 'bucket' cycles in the tension mode. The detrimental effect on the fatigue lives was already mentioned above.

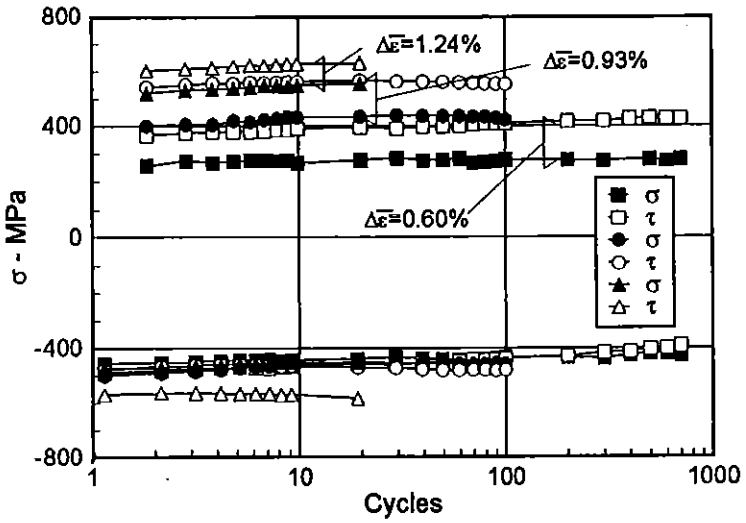

Fig. 3 Axial and torsional stress versus number of cycles for 'bucket' cycles, $\Delta\overline{\varepsilon}$ = 0.6 %, 0.93 %, 1.24 %

Temperature History Effects

A comparison between the isothermal and the sinusoidal non-proportional tension-torsion TMF responses at temperatures 450 °C to 950 °C with an effective mechanical strain of $\bar{\varepsilon} = 0.6\%$ is shown in **Figure 4.** In this figure the thick solid line represents the stress loci of the TMF tests in the σ - $\sqrt{3}\tau$ stress space and the circles the stress loci of isothermal tests under the same effective strain but at different temperatures. The experimental stress loci of the TMF and isothermal tests coincide only at the highest and lowest temperatures (600 °C to 450 °C), but discrepancies can be observed at other temperatures. The study of thermal history effects has brought out an important point about thermo-mechanical cycling. If the strain range and temperature levels activate similar deformation mechanisms, the isothermal values can be expected to model the TMF-response satisfactorily by interpolation. However, if different deformation mechanisms are activated, temperature history effects may be very important.

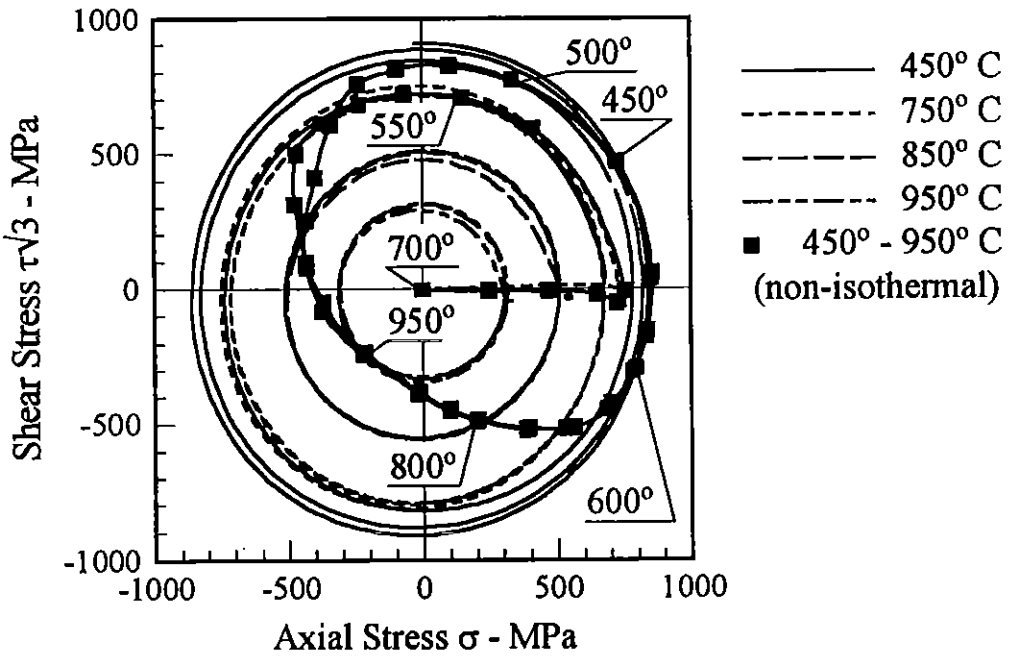

Fig. 4 Comparison of TMF and isothermal stress responses for 90° out-of-phase strain cycling, $\bar{\varepsilon} = 0.6\%$, of IN 738 LC.

Experimental Verification of the J_2-Theory for TMF Loading

The equivalent stresses and strains of simple and complex TMF loadings were calculated by the v. Mises relation, **Figure 5**. The curves of equivalent stresses versus equivalent strains lead to very complex shapes because all values are positive. Therefore the curves were changed by signs to get the usual hysteresis loops. Pure tension-compression- and torsion-tests as well as tension-compression-torsion-tests with $\varphi_T = 0$ (IP) are compared in **Figure 5 a. Figure 5 b** represents the OP-path with $\varphi_T = 90°$ and **Figure 5 c** the complex path. In this diagram the pure torsional load is left. The equivalent stress values of pure tension-compression-tests are about 100 MPa lower than the other. The deviations are inside the scatterband of this material. These diagrams verify that the v. Mises-hypothesis is altogether applicable to the deformation behaviour of IN 738 LC at TMF loading.

Life Relations for Thermomechanical Fatigue

Although numerous life prediction methods have been forwarded for simple TMF-tests (**6 – 9**), few studies were directly concerned with the fatigue life of 'bucket' TMF paths (**1**). At elevated temperatures, under cyclic loading, the inelastic deformation of metals is comprised of both plastic and viscous components. Since both plastic and viscous deformation mechanisms can serve as driving forces for microcrack initiation and propagation, cumulative fatigue and creep damage mechanisms are intimately coupled under TMF loading. The driving force for the propagation of the nucleated cracks in metals is a function of the shear and normal stresses acting on the crack plane (**10**). In multiaxial loading conditions the magnitude of the stresses depends on the strain paths. A global measure which includes all of the above mentioned parameters is the inelastic work $\sum \sigma_{ij} \Delta \varepsilon_{ij}^{in}$. Therefore the general form of the criterion is:

$$\sum \sigma_{ij} \Delta \varepsilon_{ij}^{in} = A N_f^m \tag{5}$$

where the coefficient A and the exponent m is calculated by linear regression for each TMF

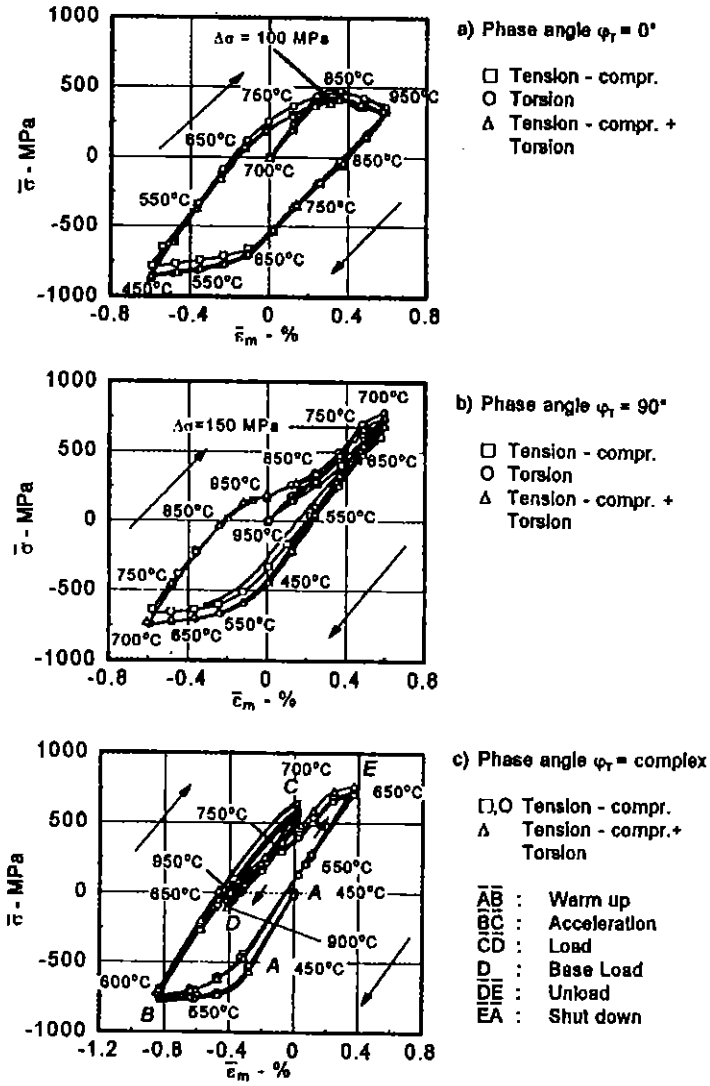

Fig. 5 Comparison of uni-and multiaxial TMF-tests (v. Mises relation) 450 °C >T > 950 °C, $\dot{\bar{\varepsilon}}_m = 10^{-4}$1/s, $\Delta\bar{\varepsilon}_m = 1.24\%$

history. **Figure 6** shows the data of five TMF histories with their straight-lines of regression. The most outside data points limit a scatterband with a N_f – width factor 2.25 with respect to the scatterband midlife. N_f was defined as the cycle at which the maximum stress dropped off to 1 % of a steady-state value including also points after saturation. As is shown in **Figure 6** the results of the uniaxial and biaxial TMF tests fall in a narrow band.

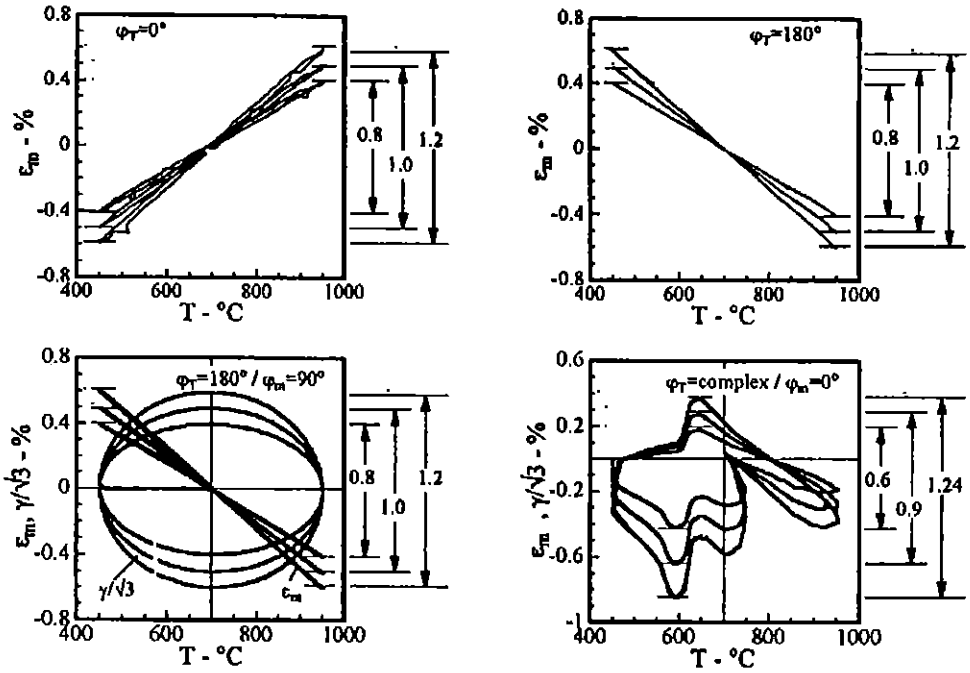

a : Identification paths ε_m/T

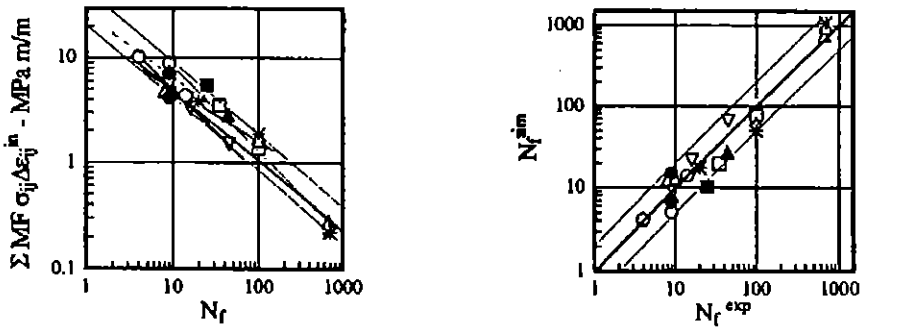

b : Determination of A, m by ID-tests.

c : Verification of A, m.

Identification (ID-) - tests

tension-compr.
- ▽ Ψ_T = 0°
- □ Ψ_T = 180°
- △ Ψ_T = compl.

tension-compr.+ torsion
- ✱ Ψ_T = compl.
- ○ Ψ_T = 180°, sinus.

Verification-tests

- ▲ Ψ_T = 90°, Ψ_m = - , ΔT = 850 - 600°C
- ◆ Ψ_T = 180°, Ψ_m = 90°, ΔT = 950 - 450°C
- ■ Ψ_T = 180°, Ψ_m = 90°, ΔT = 850 - 600°C
- ● Ψ_T = 0°, Ψ_m = 0°, ΔT = 950 - 450°C

Fig. 6 $\Sigma\sigma_{ij}\,\Delta\varepsilon_{ij}^{in}$ **versus number of cycles for different tests including applied strain paths (at the top) and simulated versus experimental life**

The quality of the lifetime prediction is also presented in **Figure 6.** As can be seen the correlation is generally within a factor of ± 2 of the medium between predicted and actual life.

Manson and Halford (11) proposed a stress based multiaxiality factor MF that modifies the inelastic work. The factor accounts for the change in ductility of a material as the state of stress changes

$$\Sigma \, MF \, \sigma_{ij} \Delta \varepsilon_{ij}^{in} = AN_f^m \tag{6}$$

where

$$MF = \frac{1}{2 - TF}, \; TF \leq 1 \tag{7}$$

$$MF = TF, \; TF \geq 1 \tag{8}$$

and

$$TF = \frac{\sigma_1 + \sigma_2 + \sigma_3}{\frac{1}{\sqrt{2}} \sqrt{(\sigma_1 - \sigma_2)^2 + (\sigma_2 - \sigma_3)^2 + (\sigma_3 - \sigma_1)^2}} \tag{9}$$

However, the equation (6) estimates the fatigue lives with nearly the same degree of accuracy as without the multiaxiality factor.

Experimental Study of the Anisotropic and Non-Homogeneous Deformation Behaviour of SC 16 Single Crystals

In order to take full advantage of Nickel based single crystal superalloys it is necessary to understand the anisotropic and non-homogeneous deformation behaviour. Therefore the local deformation characteristics of the SC 16 alloy were investigated via detailed studies of the local deformation with strain gauges at RT. The observations were analysed and interpreted in terms of crystallographic slip. In discussing TMF testing on single crystal superalloys it will be necessary to deal with non-uniform strain distribution along the circumference of different oriented tubular specimens under tension, torsion and tension-torsion loading.

Experimental Evidence of the Tensile Behaviour

The mechanical response of SC 16 alloy in a tensile test depends on material orientation, temperature, strain and specimen shape and is quite different from that of a polycrystalline alloy. Initially round tubular specimens of different diameters (26.5 mm outside diameter, 1.5 mm thickness; 20 mm outside diameter, 1.5 mm thickness) in the near [001] or within the standard triangle type orientations deform into cross sections with a complex shape, **Figure 7**. In contrast the post yield response of solid specimens shows a cross section with a circular or elliptical shape. There is not a clear explanation of this fact up to now. The reason is mainly to be found in the complexities of the deformation modes present in two-phase materials. The active deformation modes and their critical stresses depend on the composition, the temperature, the strain rate, the stress state and the previous deformation history. The work of Chin and Mammel **(12)** was the first attempt to do a systematic analysis of activated slip systems in the standard stereographic triangle. For {111} <101> slip systems, loading of fcc materials in or near the [001] direction will activate eight slip systems simultaneously if the stress is equivalent to the critical resolved shear stress (CRSS). Theoretical predictions of the combinations of active slip systems in a single crystal of a particular orientation have usually been based on one or two extreme sets of assumed boundary conditions. In the case of hollow specimens there could be particular boundary conditions on strain. The geometrical part of single-crystal plasticity is then the yield condition. This provides the basis for deriving which combination of slips will be activated among the many that are kinematically possible to achieve a given strain increment, and what particular stress state is necessary to activate this combination.

Torsion Tests on <001> Specimens at RT

Local strain measurements by means of eight strain gauge rosettes at room temperature prove that four 'soft' zones are present in the specimens near <110> and four hard zones in <100> orientations, **Figure 8**. This fact has already been mentioned by Nouailhas et al **(13)**. The simulation of such non-homogeneous test requires octahedral and cube slip.

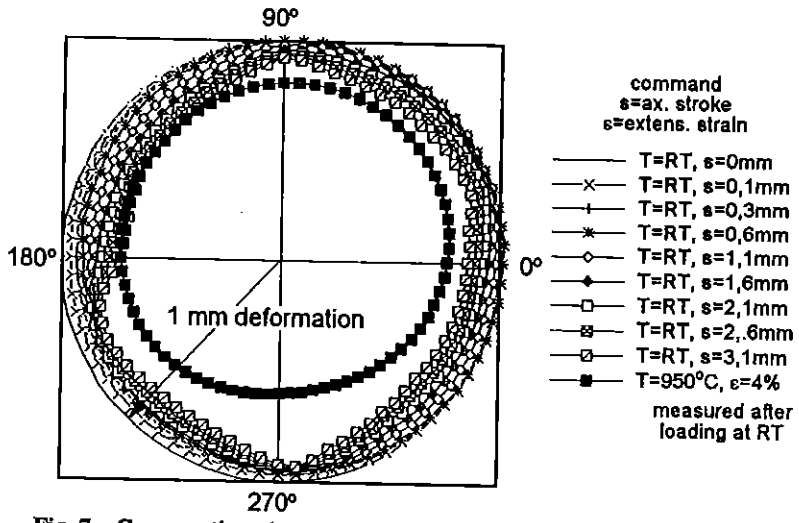

Fig. 7 Cross sections (contours) of hollow specimens at RT and T = 950 °C

Tension-Torsion Tests on <001> Specimens at RT

A completely non-symmetrical, non-homogeneous deformation behaviour is observed under tension-torsion testing on [001] oriented specimens at room temperature. Eight strain gauge rosettes were attached along the circumference as above. One of them is

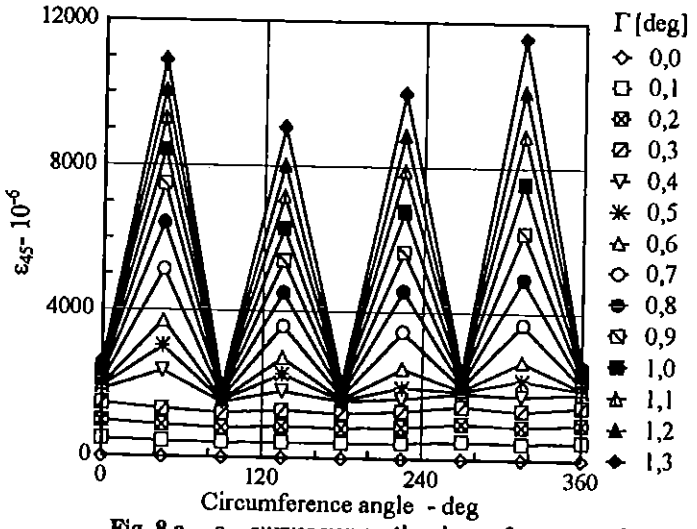

Fig. 8 a ε_{45}-curves versus the circumference angle

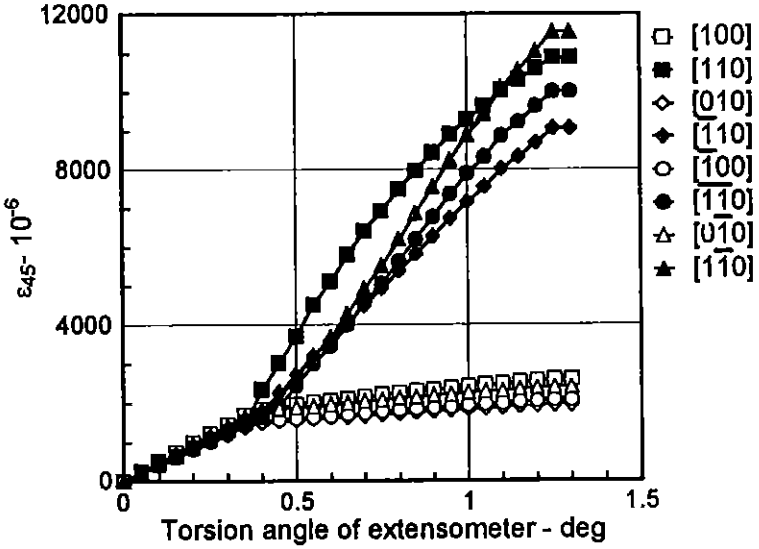

Fig. 8 b ε_{45} **– curves versus the torsion angle of the extensometer**

located near a <100> direction, the others were regularly disposed. Axial and torsional strains were also measured by means of an axial-torsional extensometer attached to the specimen near [010]. **Figure 9** shows the results of the strain gauges in the axial direction and at 45°. Different tension-torsion loading paths were measured. As can be seen in this diagram the deformation is found to be non-uniform and non symmetrical. There are two 'soft' regions. When tension becomes predominant, quasi – uniform straining is obtained only in the axial directions.

These findings were confirmed by yield surface tests, **Figure 10**. The surface was determined by following radial (proportional) stress paths from the origin with an axial-torsional extensometer attached at different positions along the circumference. A small von Mises equivalent strain offset of yielding, ~ 10^{-5}mm/mm was selected. Octahedral slip (oblique segments) and cube slip (horizontal segments) are both involved in this diagram. The experiments prove, **Figure 10 a**, that there is a non-uniform inelastic strain distribution along the circumference of <001> orientated specimens due to different slip systems (octahedral and cube slip). However, the assumption of homogeneous stresses in the specimen lead to same experimental yield surfaces, **Figure 10 b.** This diagram also confirms that a quadratic expression **(14, 15)** of a macroscopic yield criterion is not acceptable for a single crystal.

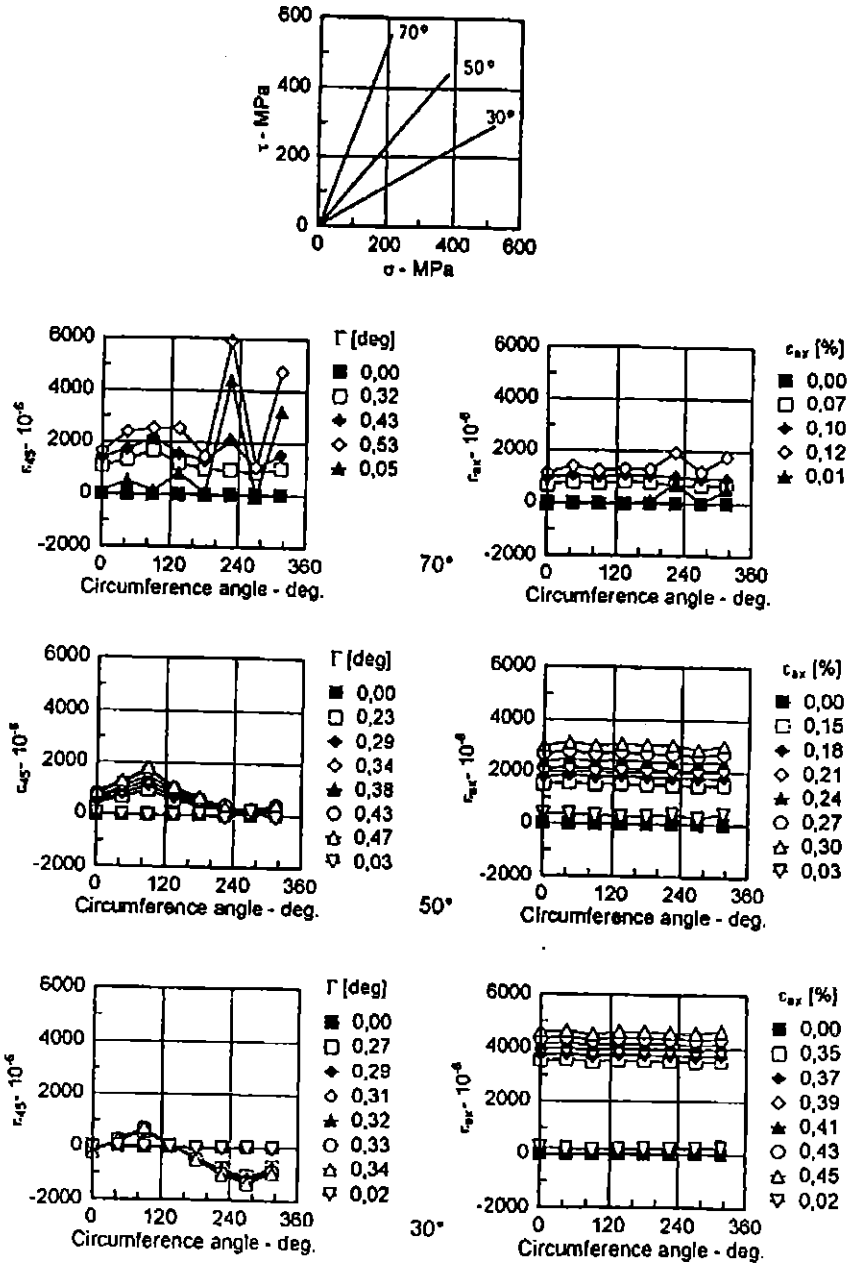

Fig. 9 Readings of eight strain gauge rosettes in the axial direction and at 45° versus the circumference angle in dependence of the loading paths 30°, 50°, 70° (at the top)

a

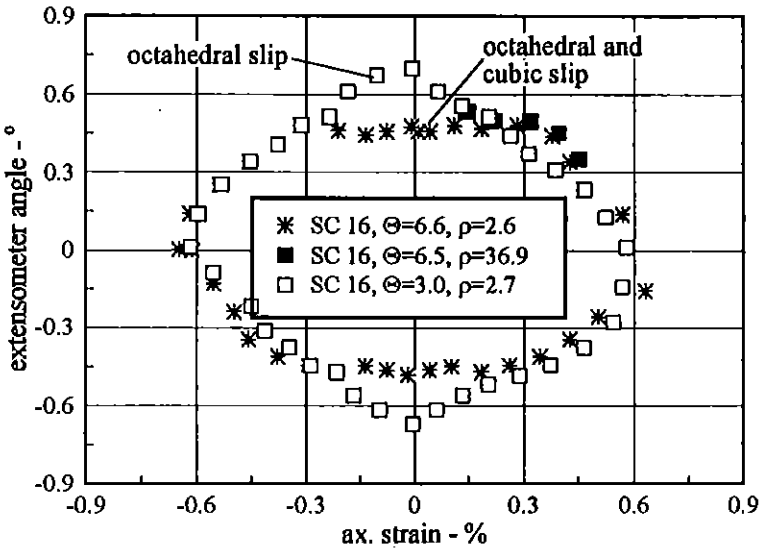

b

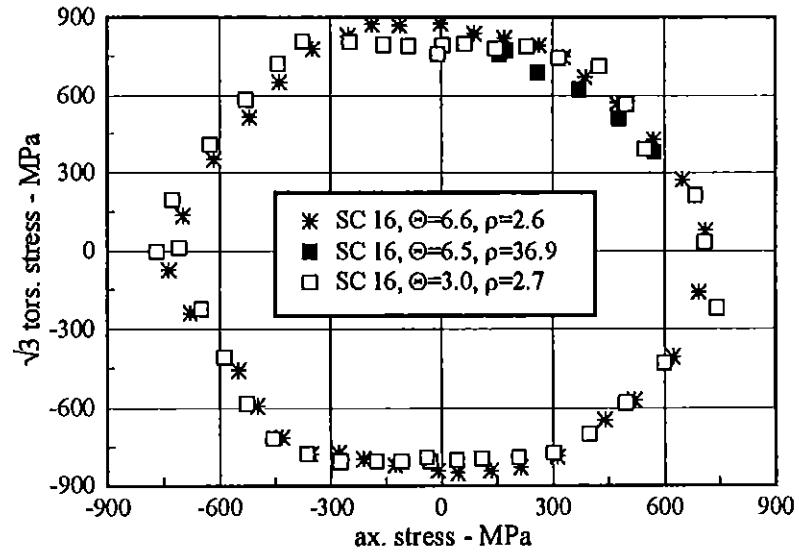

Fig. 10 Yield surfaces of a [001] oriented specimens,

a) applied axial-torsional strain paths, extensometer at different positions along the circumference
b) shear stress-axial stress plane
(Θ, ρ: orientation of the crystal axes in terms of the angles Θ and ρ in the stereographic triangle)

Conclusions

This study has demonstrated the versatility of the life prediction assessment. It can be applied to any arbitrary temperature-strain phasing. The sinusoidal TMF-time histories show the greatest inelastic works and result in the fewest cycles to failure. The scatterband with a N_f – width-factor is nearly the usual of 2.0.

It was verified by experiments that the v. Mises-hypothesis is altogether applicable to the deformation behaviour of IN 738 LC at TMF loading.

Initial experiments on single crystal superalloy SC 16 prove that there is a non-uniform strain distribution in the plastic region along the circumference of [001] orientated specimens under torsion or tension-torsion loading. This fact must be weighed when exact TMF tests are performed. The behaviour reported can be explained in terms of slip on a finite number of slip systems.

References

(1) Russel, E. S., (1986), Practical life prediction methods for thermal-mechanical fatigue of gas turbine buckets, Proc. Conference on Life Prediction for High-Temperature Gas Turbine Materials, (Edited by V. Weiss and W.T. Bakker, EPRI AP-4477, Electric Power Research Institute, Palo, Alta, CA), pp 3-1 – 3-39

(2) Kuwabara, K., Nitta, A., Kitamura, T, (1983), Thermal-mechanical fatigue life prediction in high-temperature component, Materials for power plant, Proc. of the ASME International Conference on Advances in Life Prediction Methods, Albany, NY, pp 131 – 141

(3) Bernstein, H.L., Grant, T.S. McClung, R.C., Allen, J.M., (1993), Prediction of Thermal-mechanical fatigue life for gas turbine blades in electric power generation, Thermo-mechanical Fatigue Behaviour of Materials, ASTM STP 1186 (Edited by H. Sehitoglu), American Society for Testing and Materials, Philadelphia, pp. 212 – 238

(4) Ziebs, J., Meersmann, J., Kühn, H.-J., Ledworuski, S., (1992), High temperature inelastic deformation of IN 738 LC under uniaxial and multiaxial loading, Low Cycle Fatigue and Elasto-Plastic Behaviour of Materials - LCF 3, (Edited by K.T. Rie), Elsevier Applied Science, pp. 248 – 255

(5) Meersmann, J., Ziebs, J., Kühn, H.-J., (1994) The thermo-mechanical behaviour of IN 738 LC, Materials for Advanced Power Engineering, Part I, (D. Coutsouradis et al, Eds.), Kluwer Academic Publishers, pp 841 - 852

(6) Swanson, G.A., Linask, J., Nissley, D.M., Norris, P.P., Mayer, T.G., Walker, K.P., (1987), Life prediction and constitutive models for engine hot section anisotropic materials program, NASA Report 179594, National Aeronauties and Space Administration, Washington, D.C.

(7) Remy, L., Bernard, H., Malpertu, I.L., Rezai-Aria, F., (1993), Fatigue life prediction unter thermal-mechanical loading in a Nickel-base superalloy, Thermomechanical Fatigue Behaviour of Materials for Testing and Materials, ASTM STP 1189, (H. Sehitoglu, Eds), ASTM, Philadelphia, pp 3 – 16

(8) Neu, R.W. and Sehitoglu, H., (1989), Thermomechanical fatigue, oxidation and creep: part I. Damage mechanisms, and part II. Life prediction, Metallurg. Transactions A., vol. 20 A, pp 1769 – 1783

(9) Bakis, C.E., Castelli, M.G., Ellis, J.R., (1993), Thermo-mechanical behaviour, Advances in Multiaxial Fatigue, ASTM STP 1191, (D.L. Mc Dowell and R. Ellis, Eds.), American Society for Testing and Materials, Philadelphia, pp 223 – 243

(10) Socie, D., (1993), Critical plane approaches for multiaxial fatigue damage assessment, Advances in Multiaxial Fatigue, ASTM STP 1191, (D.L. Mc Dowell and R. Ellis, Eds.), American Society for Testing and Materials, Philadelphia, pp 7 – 35

(11) Manson, S.S., Halford., G.R., (1971), Discussion, multiaxial low cycle fatigue of type 304 stainless steel, J. Eng. Mat. Techn., ASME, vol 99, pp 283 – 286

(12) Chin., G.Y., Mammel, W.L., (1967), Computer solution of the Taylor analysis for axisymmetric flow, Transactions Metallurg. Soc. AIME, vol. 239, pp 1400 – 1405

(13) Nouailhas, D., Cailletaud, G., (1995), Tension-torsion of single crystals superalloys: experiment, Int. J. Plasticity, vol. 11, No. 4, pp 451 – 470

(14) Hill, R., (1948), A theory of the yielding and plastic flour of anisotropic metals, Proc. of the Royal Society of London, Series A, pp 281 – 297

(15) Lee, D., Zaverl, F., (1978), A generalized strain rate dependent constitutive equation for anisotropic metals, Acta Metallurgica, pp 1771 - 1780

Acknowledgements

The study presented here is part of an extensive investigation into IN 738 LC and SC 16 under multiaxial states of stress and temperature history. The financial support for this research, provided by Deutsche Forschungsmeinschaft (DFG), is gratefully achnowledged.